Chemical Engineering & Technology Research Article

Marcel Loewert[1,*]
Julian Hoffmann[2]
Paolo Piermartini[2]
Manuel Selinsek[2]
Roland Dittmeyer[1]
Peter Pfeifer[1,2]

Microstructured Fischer-Tropsch Reactor Scale-up and Opportunities for Decentralized Application

Current projects focusing on the energy transition in traffic will rely on a high-level technology mix for their commissioning. One of those technologies is the Fischer-Tropsch synthesis (FTS) that converts synthesis gas into hydrocarbons of different chain lengths. A microstructured packed-bed reactor for low-temperature FTS is tested towards its versatility for biomass-based syngas with a high inert gas dilution. Investigations include overall productivity, conversion, and product selectivity. A 60-times larger pilot-scale reactor is further tested. Evaporation cooling is introduced which allows to increase the available energy extraction from the system. From that scale on, an autothermal operation at elevated conversion levels is applicable.

Keywords: Biomass-to-liquid, Compact reactor technology, Fischer-Tropsch synthesis, Microstructured reactor, Renewable fuels

Received: February 26, 2019; *revised:* April 15, 2019; *accepted:* July 09, 2019

DOI: 10.1002/ceat.201900136

1 Introduction

The heterogeneously catalyzed Fischer-Tropsch synthesis (FTS) was discovered over 90 years ago [1] to produce synthetic fuels out of syngas, CO, and H_2. Coming from coal gasification (coal-to-liquid, CtL), the FTS nowadays experiences renewed interest with novel process paths towards syngas. It offers the possibility to change the present fuel consumption while using renewables to produce synthetic fuels with distinct advantages compared to its fossil counterparts. This technology could help to lower the anthropogenic carbon footprint in the transport sector due to multiple available feedstocks (X-to-liquid, XtL). Conversion technologies range from natural gas or biogas liquefaction (gas-to-liquid, GtL) to applications using electricity, water and CO_2 (power-to-liquid, PtL) or organic sources like biomass (biomass-to-liquid, BtL).

The route from syngas to synthetic fuel (synfuel) according to a simplified reaction equation for the FTS is:

$$n\mathrm{CO} + 2n\mathrm{H_2} \rightarrow -(\mathrm{CH_2})-_n + n\mathrm{H_2O} \quad \Delta H_R^0 = -158\ \mathrm{kJ\ mol^{-1}} \tag{1}$$

Humanity will still rely on liquid fuels in the next few decades due to a lack of alternatives in certain areas, e.g., aviation [2]. State-of-the-art fossil fuels have two problems: a limited availability of global reserves with slowly decreasing product quality [3] and the critical release of CO_2 from combustion that has been chemically stored underground for millions of years, which ultimately changes the global climate [4]. The use of alternative fuels offers an important possibility to reduce the anthropogenic greenhouse gas emissions while using an existing infrastructure. This has internationally been identified.

Several initiatives and projects investigate the improvement and application of advanced technologies to change energy sources and consumption. Examples are the World Bank's "Zero Routine Flaring by 2030" initiative [5] or Germany's "Kopernikus projects" [6]. Those operations aim to establish decentralized, on-site production units, may it be near an isolated gas or oil field or the executive support of a future power grid for optimized energy distribution via sector coupling.

The flexibility of the FTS is remarkable since many carbon feedstocks can be converted into syngas. Another stand-out feature is the high volumetric energy density of the liquid product, which ranges between 40 and 48 MJ kg^{-1} [7]. Compared to fossil counterparts [8, 9], improved overall combustion properties such as lowered soot and NO_x production can be achieved due to its paraffinic nature.

Thanks to subsidies from the German government, around 36.2 % of German electricity in 2017 was generated from renewable sources such as geothermal energy, solar and wind

[1]Marcel Loewert, Prof. Dr.-Ing. Roland Dittmeyer, Prof. Dr.-Ing. Peter Pfeifer
marcel.loewert@kit.edu
Karlsruhe Institute of Technology (KIT), Institute for Micro Process Engineering (IMVT), Hermann-von-Helmholtz-Platz 1, 76344 Eggenstein-Leopoldshafen, Germany.

[2]Julian Hoffmann, Dr. Paolo Piermartini, Manuel Selinsek, Prof. Dr.-Ing. Peter Pfeifer
INERATEC GmbH, Siemensallee 84, 76187 Karlsruhe, Germany.

power or biomass [10]. An important driver of that development changed recently when fixed subsidies per unit of produced electrical energy were changed into a competitive system. Now only the most developed technologies and plants with higher efficiency are supported. This aims to further increase technological advance, cost efficiency, and competition within the renewable sector [11]. However, for a good number of existing plants this poses an insecurity for a continuous economical operation.

Upgrade of biogas for the injection in the natural gas grid is less commonly applied compared to the direct use in decentralized combined heat and power (CHP) units for local energy supply, mainly due to the high investment cost for gas cleanup.

A promising option for biomass utilization is the conversion of the feedstock into liquid energy carriers for the use as fuels or platform chemicals. Potential process steps are biomass pretreatment, gasification, gas cleaning, and FTS with power generation from the gaseous FT byproducts and FT liquids [12]. Today, bioenergy contributes to approx. 50 % of all renewable energy that is consumed worldwide [13].

FTS in the framework of biomass conversion may be one important technology if the goals of the Paris agreement are to be kept by 2050. Besides FTS, BtL processes are able to produce different liquid energy carriers. Target products can include ethanol, methanol, dimethyl ether (DME), oxymethyl ether (OME), or methanol-to-gasoline (MTG) products. Already existing or soon to be commissioned BtL pilot-plant projects in Europe producing advanced biofuels include BioDME (DME synthesis, Chemrec, Sweden), Bioliq (methanol, DME, gasoline, KIT, Germany), Güssing FT (renewable diesel on gasifier side stream, Vienna University of Technology/BIOENERGY 2020+, Austria), and BioTfueL (biokerosene, a French industrial consortium, France). Another BtL application can be found in Canada (ethanol/methanol, Enerkem) [14].

For industrial application, there are a number of volatile variables that make investments in large plants risky: the final product price which strongly depends on the political framework and available supply chain, the feedstock capacity, but also the current metal price and all costs concerning the feed gas supply [15]. Reducing this complexity, intensifying the process by new technologies and markets rather than increasing centralized plant sizes can be a promising strategy [3, 16, 17].

The significance and the potential of small-scale applications has recently been acknowledged. PtL demonstration projects were formed, such as PowerFuel [18] or Soletair [19]. BtL projects such as COMSYN within the Horizon2020 frame by the European Commission [20] have also been introduced. Since the total carbon footprint from the transport sector has not changed since 1990, BtL and PtL will be an effective measure towards greenhouse gas (GHG) neutral transportation and boosting the bio-share quota of refineries while using an established infrastructure [21]. Car engines, fueling stations, and refineries can be further used.

A mixture of a few large plants and many decentrally applied technologies may reform the energy market of the future. Therefore, PtL/BtL plants are considerable building blocks for energy conversion. Different scenarios focus already on applications in the heavy transport sector, e.g., shipping and aviation [22, 23].

Due to the highly exothermic properties of the FTS, the conversion in common industrial reactors needs to be limited to avoid hot spots that would permanently harm the catalyst [24]. Because of this limited conversion, the product gas, which is rich in unconverted feed gas components, needs to be recycled in order to reach high carbon efficiency. This leads to increased cost [25]. Typical approaches to reduce hot spots are further dilution of the catalyst in the formed liquid phase in slurry-bed reactors or via egg-shell catalysts in tube-bundle reactors. Since it matters strongly how well the reaction heat can be taken out of a system, microstructured reactors show big advantages in this regard [26].

Heat removal from the catalyst and mass transfer from gas via the formed liquid phase to solid catalyst are intensified within microstructures, allowing to manage the active site temperature to stay isothermal even under challenging process conditions such as conversions around 80 % [27–29]. The possibility of a high conversion reduces or even omits gas recycling and thus simplifies the overall process. Due to intensified mass transfer, a very high space-time yield, which is nearly 100 times larger compared to conventional slurry-phase reactors, can be reached. A compact and modular plant design with small footprints can therefore be realized (see Tab. 1). This simplified, compact, and modular setup potentially enables decentralized application such as offshore or remote solutions [23, 30].

Previously inaccessible markets open up by utilizing locally available feedstocks [17]. Industrial application of microstructured reactors is often restrained due to less confidence in the technology. Scaling-up can be achieved by simple multiplication of microstructures [31]. In the area of FTS, advanced reactor technology is already bridging the gap between academia and industry [32–35].

Table 1. Comparison of intensified FTS technology in demonstration or industrial scale with conventional reactor systems, as well as catalyst activity from literature [36–38].

	Catalyst activity (C5+ per catalyst mass) [$g_{C5+} g_{cat}^{-1} h^{-1}$]	Space-time yield (C5+ per reactor volume) [$kg\,m^{-3} h^{-1}$]
INERATEC®	2.1	1785
Velocys	–	1600
Oryx GTL – Sasol	–	20.6
Literature review	1.4	–

Fischer-Tropsch products consist of linear and branched alkanes (paraffins, iso-paraffins), alkenes (olefins), and oxygenates. The products come in gaseous, liquid, and solid form under ambient conditions. The selectivity towards species and carbon chain length in the product mixture is strongly dependent on adjusted process conditions. Most important are temperature, residence time, partial pressures, and the catalyst system itself. Due to cleaned feed syngas from purification, the final fuels do not contain any organic sulfur or aromatics and have a cetane number well above 50 [24]. A high dilution with nitrogen is likely for any biomass-based feed from

gasification or for biogas using air instead of oxygen for gas reformation [39].

In this work, influences from the feedstock on product properties are highlighted for the low-temperature FTS (LTFT). A previously introduced microstructured fixed-bed reactor is used [28, 40]. Different microstructured layouts are tested and optimized towards their effect on product properties in pure syngas before [29]. There, the high surface area of the reaction foils has been found to be very effective in removing the reaction heat. Thermal stability under severe conditions has also been demonstrated before [28].

The present study details the influence of different partial and total pressure levels, as well as H_2/CO ratios. A thorough analysis of all product fractions is executed. Furthermore, a scaled-up pilot reactor is tested which allows comparison of results with the much smaller lab-scale reactor at varying system temperature and weight hourly space velocity (*WHSV*). Due to autothermal behavior within this reactor scale, evaporation cooling is introduced as the method of choice to extract the released reaction enthalpy from the system and to efficiently change the system temperature. Similar process conditions are tested for both reactor scales to evaluate possible effects from feed gas dilution in order to simulate syngas from BtL applications.

2 Experimental

2.1 Catalyst

For all featured experiments, a commercial cobalt catalyst with 20 wt % Co and 0.5 wt % Re on an optimized γ-alumina support was used. Cobalt is the preferred catalyst for LTFT if saturated compounds are targeted. It shows high selectivity towards linear alkanes, a high activity at low temperature as well as a negligible water-gas shift (WGS) activity compared to iron catalysts [3, 41, 42]. The particle size distribution was adjusted to 50–200 µm for the fixed bed inside the microstructures.

Approximately 2 g and 120 g of catalyst were placed inside the lab and pilot reactor, respectively. The catalyst was first reduced in situ with either heat transfer oil flowing through the cooling channels or heat cartridges placed on top of the reactor surface. A temperature ramp for the reactor surface was applied starting from room temperature to 623 K with 1 K min^{-1}. For that ramp, a gas mixture of 5 % H_2 and 95 % N_2 was given to the reactor. The final temperature was held for 16 h. Once the temperature maximum was reached, 100 % H_2 was fed into the reactor for the rest of the reduction. After 16 h, the reactor was cooled down to 443 K. From that temperature the different reaction parameters and gas flows were adjusted.

2.2 Microstructured Reactors

2.2.1 Lab Scale

The reaction was carried out in a microstructured reactor that has been applied previously [28] and consecutively optimized regarding its structural properties [29]. The principal functionality has been elaborated. Negligible pressure drop in the reaction on the fixed bed was found due to appropriate particle sizes and reactor layout [43].

The reaction volume of the applied system was 2.71 cm^3 formed by eight diffusion bonded reaction foils containing micropillars with 0.75 mm height and 1.2 mm space between each other in face-to-face arrangement to form four reaction slits. Temperature control was ensured by five structured foils, which were stacked in between the reaction slits and where heating oil (Therminol 66, Fragol) was pumped through. The temperature at inlet and outlet of the reaction was measured with temperature sensors placed in the foil stack.

2.2.2 Pilot Scale

The larger pilot-scale reactor was designed with a scale-up factor of around 60 compared to the reactor described in Sect. 2.2.1 (Fig. 1). The foils were redesigned and optimized to fit the larger outer dimensions. The new development results in a reaction volume of ca. 163.4 cm^3 which was designed for at least 6 L of product per day, depending on process conditions. Additionally, channels with specially designed cooling structures were integrated for water entering at nearly boiling temperature. Evaporation cooling should keep the reaction temperature isothermal.

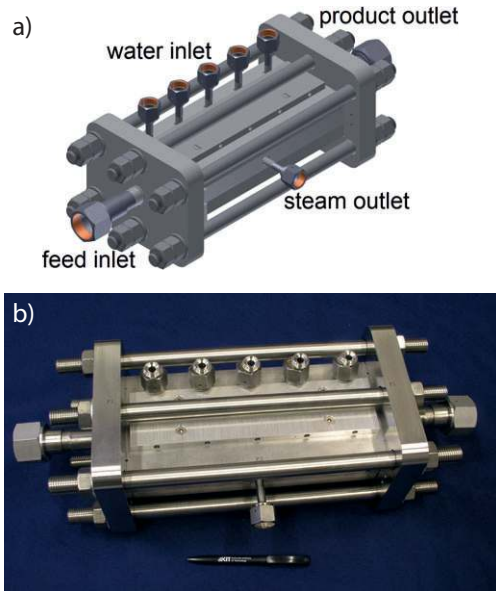

Figure 1. CAD sketch of the pilot-scale reactor (a) and a photo of the resulting design with a pen for size comparison (b).

2.3 Reaction Setup

The periphery of the smaller reaction setup was described earlier [29, 44]. The larger system showed the same structural properties but with associated bigger product traps and an evaporation cooling cycle under pressure (Fig. 2).

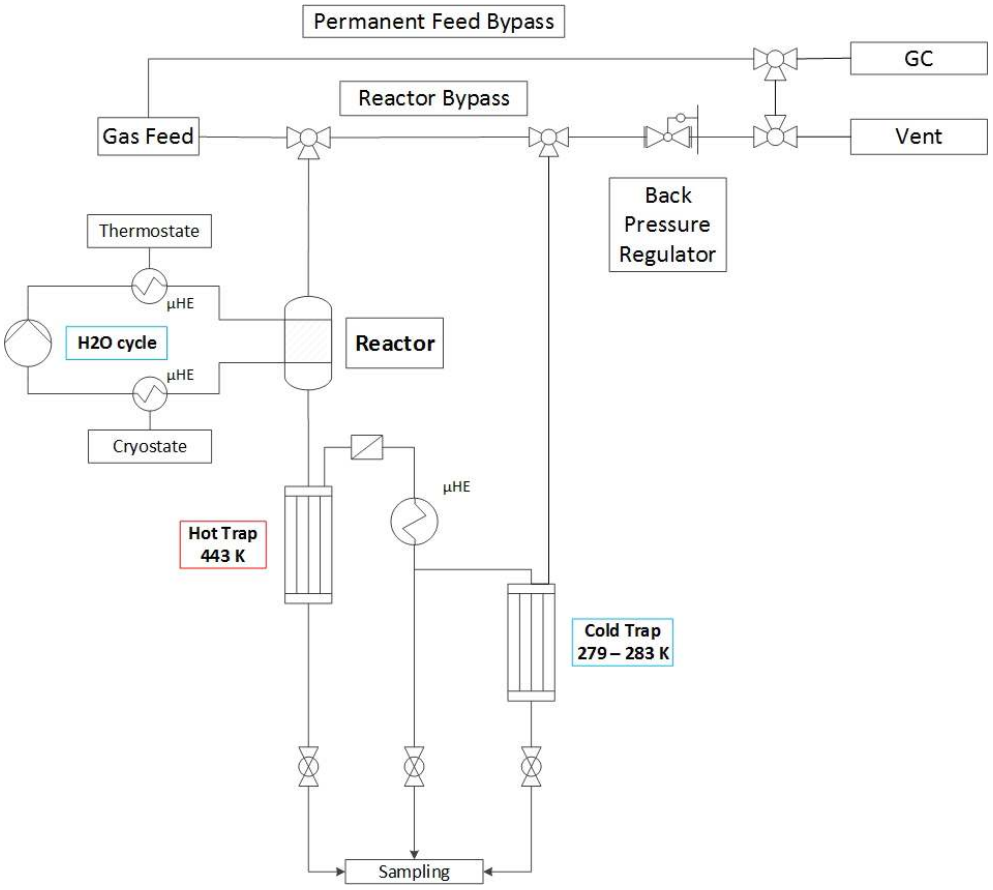

Figure 2. Overview of the pilot-scale reaction setup; a small amount of the gas mixture is bypassing the reactor to measure the feed (labeled Permanent Feed Bypass) via GC analysis. A micro heat exchanger (labeled µHE) is used to condense the liquids for the cold trap.

The feed gas supply was regulated by mass flow controllers (MFCs; model 5850S, Brooks) and monitored by a mass flow meter (MFM; model 5860S, Brooks). All tubing material and system components such as valves and pressure regulators were made from stainless steel. This material meets the respective requirements regarding operating pressure and temperature and shows no interaction with the reactants. Liquid products were first collected in a hot trap, which is a pressure resistant container with a volume of about 4 L. It was electrically heated to 443 K for that higher hydrocarbons, the so-called wax, can condense in this vessel. The subsequent cold trap was held at low temperature to collect the condensed and residual liquefiable product fraction from the micro heat exchanger. This vessel is the largest system component with about 20 L of total volume which is kept below 300 K by a stainless-steel cooling coil of about 2 m length inside the vessel.

The liquefied product accumulated in the respective trap system for offline sampling while the gaseous fraction of the product was led to an online GC system (Agilent 6890N) to determine the conversion and selectivity towards gaseous components. The system pressure was held by a back pressure regulator valve. A permanent bypass with a low flow was adjusted with a fine needle valve to measure the feed gas composition.

2.4 Product Analysis

All three product phases demanded their own method of analysis, all of which needed to be carried out in different GC systems. Products formed gaseous or liquid at reaction conditions. The wax fraction removed from the hot trap under liquid conditions needed to be melted and dissolved after sample solidification. A liquid "oil" fraction accumulated inside the cold trap with accompanying water. The water was separated from the upper, nonpolar phase before analysis. Liquid products were analyzed with a 7820 GC (Agilent) in a DB–2887 column (Agilent), while the solid fraction was analyzed using a cooled injection system and a high–temperature simulated distillation column (see Sect. 2.4.3). All samples were taken few hours after parameters were changed and after emptying the traps in between setups.

2.4.1 Gaseous Species

For gas analysis, different GC columns and detectors were applied within the unit (Agilent 7890B). Hydrocarbon species were analyzed in a flame ionization detector (FID), while a thermal conductivity detector (TCD) was used to measure H_2, N_2, O_2, CO, and CO_2 as well as hydrocarbons up to heptane. Two HayesepQ columns (Agilent) first separated hydrocarbons

from CH_4 to C_7H_{14}, as well as CO_2 from the rest of the permanent gases. Two Molsieve 5A columns (Agilent) were used to split the retained CO, N_2, and H_2, while a PoraPlot Q column (Agilent) separated the hydrocarbons and CO_2.

By measuring a feed bypass, the present H_2/CO ratio could be calculated via the gas fraction y_i[1]:

$$\frac{H_2}{CO} = \frac{y_{H_2,feed}}{y_{CO,feed}} \tag{2}$$

Syngas conversion X_i was determined using nitrogen as internal standard to correlate the flow before and after the reaction, since there is considerable volume reduction from the reaction. The conversion can be calculated according to:

$$X_{CO} = \frac{\frac{y_{CO,feed}}{y_{N_2,feed}} - \frac{y_{CO,product}}{y_{N_2,product}}}{\frac{y_{CO,feed}}{y_{N_2,feed}}} \tag{3}$$

The selectivity of hydrocarbon components was determined by means of an FID detector. N_2 was only detected on the TCD. Since CH_4 was measured on both detectors, the relation of its signal between FID and TCD was taken as an additional factor:

$$S_{C_iH_x} = \frac{i\frac{y_{C_iH_x,FID}}{y_{N_2,product}}\frac{y_{CH_4,TCD}}{y_{CH_4,FID}}}{\frac{y_{CO,feed}}{y_{N_2,feed}} - \frac{y_{CO,product}}{y_{N_2,product}}} \tag{4}$$

with i being the carbon number and x being the equivalent number of hydrogen atoms of the observed hydrocarbon. The selectivity towards products with carbon chain lengths of five and higher ("fuel range") was determined by subtracting the selectivity towards gaseous components from 1:

$$S_{C_{5+}} = 1 - \sum_{i=1}^{4} S_{C_iH_x} \tag{5}$$

2.4.2 Liquid Product

Under ambient conditions, the liquid phase from the cold trap consists of a lower water phase and a hydrocarbon phase. Many different species of molecules are present in this mixture, ranging from linear alkanes over double-bonded alkenes to branched iso-alkanes and alcohols. A GC method was applied to separate the species. Since calibration of all components is not possible due to missing standards, the correlation between the GC signal area and the number of $-CH_2-$ monomers per molecule was employed to calculate the concentration of higher hydrocarbons.

The productivity P_X was calculated for each liquid (water, hydrocarbons) and solid product. It was measured gravimetrically after an experiment via the weighed product mass m_X, with X being water, oil or wax, respectively:

$$P_X = \frac{m_X}{\Delta t m_{cat}} \tag{6}$$

After weighing and analyzing a fraction, the total amount of a chosen compound with given carbon number w_i was determined in dependence of the respective mass flows $\dot{m}_i$, gas fractions, volume flows $\dot{V}_i$, productivities and densities ρ_i:

$$w_i = \frac{\dot{m}_i}{\dot{m}_{total}} = \frac{y_i P_X m_{catalyst}}{\dot{m}_{gas} + \dot{m}_{liquid} + \dot{m}_{solid}} \text{ for solids/liquids} \tag{7}$$

$$w_i = \frac{y_i \dot{V}_{feed,STP} \rho_{i,STP}}{\dot{m}_{total}} \text{ for gaseous species} \tag{8}$$

2.4.3 Solid Fraction

Analysis of hydrocarbons with a high density and low solubility is a difficult task [45]. A method with carbon disulfide (CS_2) was applied, which showed sufficient solvent characteristics [46] and was used for analysis despite its high toxicity and low boiling and ignition point. Additionally, a separately heated injection module (Gerstel KAS 4 with C506 controller) was employed on an Agilent G1530A GC with a column that was specifically suitable for simulated distillation (Restek MXT-1HT).

2.4.4 Anderson-Schulz-Flory (ASF) Distribution

The ASF chain length distribution was originally developed by Schulz and Flory and is widely applied for FTS analysis [64]. Through Eq. (9), the so-called chain-growth probability α can be determined in the range from 0 to 1. It can be used to reflect the tendency of the catalyst to produce longer hydrocarbon chains.

$$\alpha_{(j-i)} = \exp\{-a_{j-i}\} = \exp\left\{-\frac{w_j/C_j}{w_i/C_i}\right\} \tag{9}$$

with $j > i$; i, j being the carbon chain numbers, a the slope of a linear part of the ASF plot between $x = [i\ j]$, w_x the mass fraction of chain length x, and C_x the carbon number within chain length x.

2.5 Parameter Sets

As literature implied [47, 48], there are four main process parameters having the strongest influence on the outcome of the reaction: pressure, H_2/CO ratio, temperature, and residence time. Apart from that, many different materials such as support, promotor, active metal, distribution, composition etc. may be further mentioned.

1) List of symbols at the end of the paper.

It was important to observe the system's behavior for different cases of gas composition, namely, a diluted syngas with high amounts of N_2 and or CO_2 as one would expect from biogas origins or from gasification without an air separation unit (ASU) [49].

Experiments concerning the addition of CO_2 in the feed were executed to confirm, apart from all other information, the influence of the WGS reaction on the cobal-based catalyst. This is generally reported to be negligible, depending on the catalyst system [50, 51]. Samples with running number "1" were carried out in the lab-scale reactor described in Sect. 2.2.1. Experiments with number "2" in front were carried out in the pilot-scale reactor described in Sect. 2.2.2.

The total system pressure may influence operation costs [12]. Especially in solid feedstock applications, e.g., direct biomass gasification, a higher pressure may be disadvantageous. To investigate a certain flexibility towards syngas generation, different total pressures were applied. According to literature, the total pressure exhibits no clear trend on the synthesis outcome [52, 53]. It is maybe more important to look on the partial pressure of the components, especially for gases whose presence favors deactivation [41, 53, 54]. In Tab. 2, three parameter sets regarding the pressure influence applied in the present study are listed.

The H_2/CO ratio determines the stoichiometric availability of hydrogen to form hydrocarbons with CO monomers. In biomass applications, a variety of different syngas ratios are reported depending on the gasification conditions and oxidation ratio (oxygen/air and steam content). To highlight the versatility of the reactors, different syngas ratios were tested.

Many mechanisms on how to perform the FTS "polymerization reaction" have been published in the past [54–56]. In the end, the availability of hydrogen in the catalyst bed determines whether or not chain progression can be initiated, influencing the average length of the product's hydrocarbon chain. The stoichiometric feed ratio for maximum conversion nevertheless accounts to ~ 2.15 [41].

Tab. 3 shows the two parameter sets for different H_2/CO ratios with rather unfavorable values, which may represent biomass gasification without syngas conditioning.

Syngas conversion is strongly related to the reaction temperature. However, it may also severely influence the chain length, so a parameter set should represent conditions where an acceptable low methane selectivity and sufficient CO conversion can be found. The following experiments were chosen to further investigate evaporation cooling of the microstructures in pilot scale.

Up to around 523 K, many sources describe the process as LTFT that may use iron or cobalt as an active component [57, 58]. Under those conditions, the usage of a cobalt-containing catalyst is possible since oxidation is a negligible factor for long-term activity. A high temperature would lead to shorter hydrocarbon chains, since chain termination is promoted through hydrogenation and other effects [59]. A high temperature would also enhance deactivating effects such as coking, sintering, or wax fouling [51, 60]. Three different sets of parameters with different temperatures for the pilot-scale reactor were chosen for comparison between 493 K and 513 K, as summarized in Tab. 4.

The flow rate of the gaseous feed determines the contact time with the catalyst surface. Thus, the possibility of chain growth will decrease with increasing *WHSV* since it relates the feed's (mass) flow with the mass of catalyst inside the reactor.

$$WHSV = \frac{\dot{m}_{\text{feed}}}{m_{\text{catalyst}}} \tag{10}$$

To test the pilot-scale reactor in this regard, Tab. 5 gives an overview of the process parameters chosen for a comparison.

3 Results and Discussion

3.1 General Process Properties, Analysis Results, and Stability

CO conversion was typically above 50 % in the experiments, which were carried out under high dilution. A rather large number of set points was applied in a short time, so that long-term deactivation effects could be neglected in the observed time frame. Furthermore, an initiation phase was passed, after which natural deactivation was very low. The conversion change during initiation due to catalyst reshaping is known to appear in the course of the first few hundred hours of operation [61]; liquid hydrocarbons start to fill the catalyst pores and induce diffusion limitation until a stationary conversion level is reached [62].

The conversion over time-on-stream (TOS) for the lab reactor system is depicted in Fig. 3. At every point marked with an asterisk, a parameter change was applied. Gaps in the graph are caused by feed gas measurements

Table 2. Experiments 1A–1C for varying total pressure setups in the lab-scale reactor.

Sample	H_2 [vol %]	CO [vol %]	N_2 [vol %]	CO_2 [vol %]	H_2/CO ratio	Total flow [$mL_N min^{-1}$]	*WHSV* [$g\,g^{-1}h^{-1}$]	p_{total} [MPa]	*T* [K]
1A	27.77	16.13	43.28	12.82	1.72	640	20.80	3	513
1B	29.44	16.70	42.56	11.30	1.76	640	20.18	2	508
1C	27.69	16.55	42.34	13.42	1.67	640	20.90	1.5	513

Table 3. Experiments 1A and 1D for different syngas ratios in the lab-scale reactor.

Sample	H_2 [vol %]	CO [vol %]	N_2 [vol %]	CO_2 [vol %]	H_2/CO ratio	Total flow [$mL_N min^{-1}$]	*WHSV* [$g\,g^{-1}h^{-1}$]	p_{total} [MPa]	*T* [K]
1A	27.77	16.13	43.28	12.82	1.72	640	20.80	3	513
1D	25.56	16.68	44.55	13.22	1.53	690	23.50	3	513

Table 4. Experiments 2A–2C for different temperatures adjusted within the pilot-scale reactor.

Sample	H_2 [vol %]	CO [vol %]	N_2 [vol %]	CO_2 [vol %]	H_2/CO ratio	Total flow [$mL_N min^{-1}$]	*WHSV* [$g g^{-1} h^{-1}$]	p_{total} [MPa]	*T* [K]
2A	29.46	15.41	43.47	11.76	1.91	38 147	20.08	3	496
2B	29.46	15.41	43.47	11.76	1.91	38 166	20.09	2.8	502
2C	29.46	15.41	43.47	11.76	1.91	38 166	20.09	2.8	511

Table 5. Experiments 2D and 2E with different *WHSV* in the pilot-scale reactor.

Sample	H_2 [vol %]	CO [vol %]	N_2 [vol %]	CO_2 [vol %]	H_2/CO ratio	Total flow [$mL_N min^{-1}$]	*WHSV* [$g g^{-1} h^{-1}$]	p_{total} [MPa]	*T* [K]
2D	31.08	15.47	42.02	11.44	2.01	38 134	19.65	3	499
2E	31.08	15.47	42.02	11.44	2.01	26 407	13.61	3	497

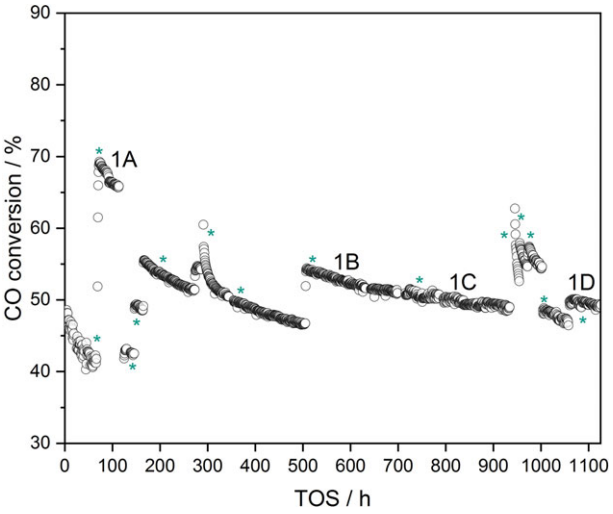

Figure 3. CO conversion over TOS for the course of over 1100 h for the lab-scale microstructured reactor with changing process parameters, each marked with an asterisk. All parameter sets described in this work are additionally labeled from 1A to 1D in the figure.

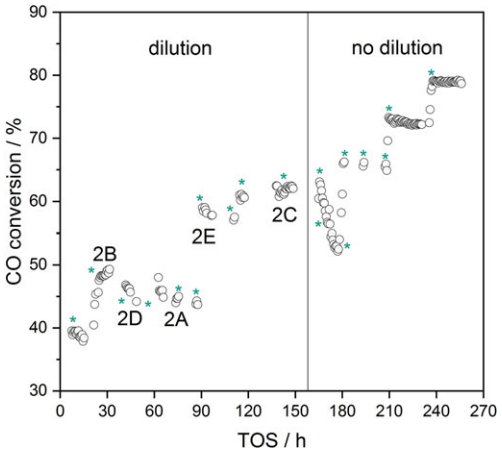

Figure 4. CO conversion over TOS of around 250 h for the pilot-scale microstructured reactor with changing process parameters, each marked with an asterisk. Setups 2A to 2E are additionally labeled within the figure. From around 155 h of TOS, experiments continued without inert gas dilution.

of the bypass instead of the product stream. The general negative slope is caused by the above-mentioned initiation of the reaction. The flattening of the conversion curve is observable after around 650 h TOS.

The lab-scale reactor behaved isothermal, meaning a temperature gradient of below 2 K, both in axial and radial length. This was observed with two thermocouples along the reactor's width and four thermocouples at the entrances and exits of both fluid streams, respectively. The efficiency of temperature regulation in this scale is very well adjustable with the use of heating oil.

In pilot scale, a maximum temperature gradient along the catalyst bed of 4 K maximum, in most cases around 1–2 K, is considered nearly isothermal. The possibility to cooling down and control the reaction temperature by evaporating water gave options to adjust temperatures in the process quickly and efficiently. The point from which the reaction behaved autothermal was reached around 35 % of CO conversion for most given flows.

In Fig. 4, CO conversion over TOS is depicted for around 250 h of experiments; an initiation phase as in the case of the lab reactor was not possible due to the considerable gas consumption of the system. Every change of parameters is marked with an asterisk. After around 155 h of TOS, several experiments without inert gas dilution were carried out, which led to an increase in CO conversion to around 80 %.

It is worth mentioning that no WGS activity was observed throughout the course of the presented experiments, as expected from cobalt systems without MnO support [63, 64]. No effect from water regarding reaction inhibition or permanent deactivation could be detected.

In Tab. 6, relevant results of all product phases are presented. CO conversion and product selectivity were calculated from the concentrations in gaseous phase averaged over TOS for each experiment.

Alkane, alkene, and iso-alkane contents were determined from the liquid product phase. The compound class spread for alkanes:alkenes:iso-alkanes was roughly 75:10:15 for lab scale and 80:10:10 for pilot scale, respectively, with ± 5 % deviation. The selectivity towards C_{5+} accounted between 66 and 83 mol %. With the given GC system, errors in the detection of alcohols might occur due to distinct overlapping with

Table 6. Overview of results for all experiments in both reactor scales.

Sample	X_{CO} [%]	P_{total} [g g^{-1}h^{-1}]	P_{wax} [g g^{-1}h^{-1}]	P_{oil} [g g^{-1}h^{-1}]	S_{C1} [mol %]	S_{C2} [mol %]	S_{C3} [mol %]	S_{C4} [mol %]	S_{C5+} [mol %]
1A	62.05	0.765	0.140	0.625	15.66	2.75	4.86	5.59	71.14
1B	58.66	1.103	0.223	0.880	14.63	2.45	4.56	5.50	72.86
1C	55.91	0.590	0.046	0.544	17.69	3.27	5.59	6.53	66.91
1D	50.86	0.739	0.119	0.620	10.84	2.85	3.99	0.19	82.13
2A	44.05	0.447	0.086	0.361	13.90	1.61	4.22	4.76	75.51
2B	47.17	0.541	0.103	0.438	14.14	1.66	4.31	4.69	75.20
2C	59.93	0.650	0.121	0.529	17.82	2.14	4.80	6.27	68.96
2D	48.87	0.494	0.094	0.400	17.10	2.08	4.84	6.95	69.02
2E	57.22	0.513	0.098	0.415	15.14	1.78	4.59	5.62	72.87

iso-alkane signals in the oil phase, making definitive identification difficult. Part of the detected iso-alkanes could therefore be alcohols.

3.2 Evaporation Cooling in Pilot Scale

The efficiency of the evaporation cooling structures was initially tested with heating oil replacing the reaction mixture in an even larger pilot reactor than presented (five times the width of the reaction zone). Preheated oil at 518 K (Therminol 66, Fragol) was put through the reactor from bottom to top to guarantee an even flow of the viscous liquid through the structures. Water was distributed from right to left inside the cooling channels by a pump with four horizontally movable thermocouples (position A–D in Fig. 5) measuring the local temperatures inside the structure. Four positions in width with even distribution were chosen (position 1–4). The observed temperature distribution is illustrated in Fig. 5 for the non-insulated reactor (a) and after insulation (b). Insulation lowered the maximum temperature gradient at the edges of the reactor at all positions, but also increased the average temperature inside the system. A gauge glass at the exit of the steam outlet was used to determine if water was fully evaporated upon leaving the reactor.

By establishing the cooling cycle with reaction media shown in Fig. 2, the system temperature was even better manipulated by the pressure of the liquid cooling medium. The relation between water pressure and boiling temperature opened a control window in which the fluid was sufficiently extracting reaction heat without extinction of the operation.

The pressure-dependent boiling temperature is held from the boiling point (saturated liquid) over the two-phase region of wet steam to the vapor region where water is fully evaporated and starts overheating. For best temperature control, the wet steam should not fully evaporate. The specific heat capacity of steam is more than 22 times lower compared to that of the liquid water. The gauge glass implied that water never evaporated completely and remained in the wet steam region. This was confirmed by temperature measurements at the steam outlet with regards to the applied water pressure. A pressure between 15 and 30 bar was adjusted to reach temperatures between 474 K and 514 K, in good agreement with the Antoine equation for water in that regime [65].

The possibility to use evaporation cooling is determined by the layout and dimensioning of the cooling channels. The

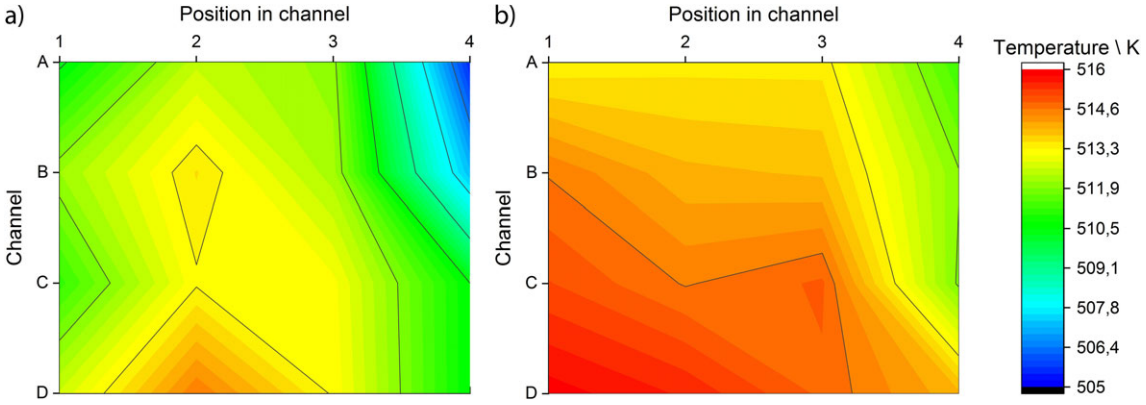

Figure 5. Temperature profile for 16 measurement spots in four thermocouple channels for a non-insulated (a) and an insulated microstructured pilot-scale FT reactor (b), as described in [26].

piping material determines the pressure that is applicable in a system. For the means of this experiment, 35 bar was chosen to be the highest applicable water pressure for which the piping was initially tested by pressure tests with nitrogen.

3.3 Total Pressure Variation in Lab Scale

As mentioned above, the effect of the total pressure on the outcome of FTS follows no certain tendency in literature. In Fig. 6, the ASF curves of three similar parameter sets at different total pressure are indicated. The total amount of methane is similar but has a trend to higher values at lower pressure. The clearest effect is on CO conversion, where the highest pressure could lead to the highest resulting value. The general forms of the ASF curves are similar except for the higher chain lengths from C_{35+} where a higher pressure is advantageous.

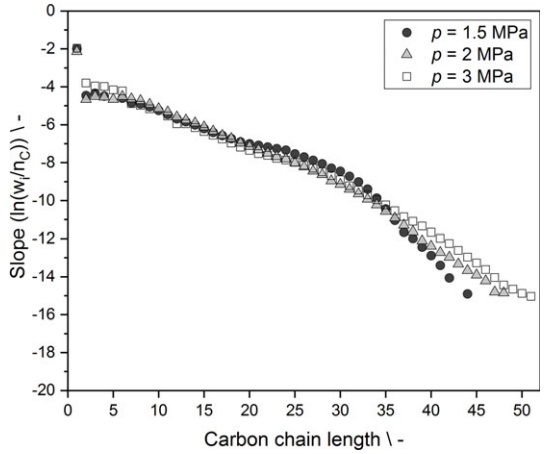

Figure 6. ASF plots for different absolute pressures and their effect on the product distribution from experiments 1A (3 MPa), 1B (2 MPa), and 1C (1.5 MPa).

3.4 H_2/CO Ratio Variation in Lab Scale

Investigations about the influence of the H_2/CO input ratio on the product distribution in regular plug-flow reactors show that the smaller the input ratio, the longer the average chain length becomes [47, 54, 66]. The expected change of chain growth probability, however, is not very distinct for the present experiments (Fig. 7). The effect of a higher dilution with nitrogen in the feed gas could have a more pronounced impact on chain termination than the available H_2/CO ratio. The chain growth probability for a H_2/CO ratio of 1.72 for C_{11} to C_{25} accounts to α_{11-25} (1A) = 82.5 %, whereas for a H_2/CO ratio of 1.53 the chain growth probability resulted in α_{11-25} (1D) = 84.0 %.

3.5 Temperature Variation in Pilot Scale

The temperature plays an important role on reaction kinetics. It is also known to determine chain termination [47, 66, 67].

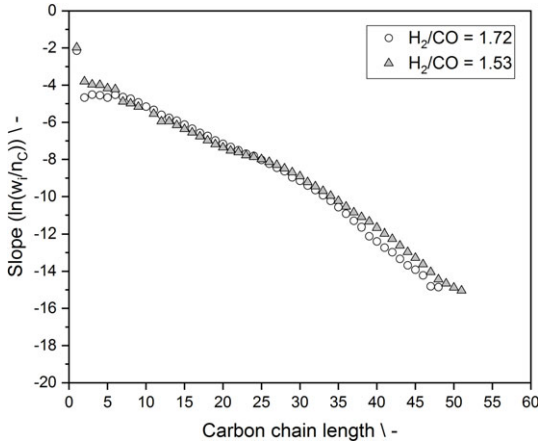

Figure 7. ASF plots with different syngas ratios from experiments 1A (H_2/CO = 1.72) and 1D (H_2/CO = 1.53).

Keeping that in mind allows a certain controllability to the process by controlling the temperature [37]. At 473 K, very weak catalyst activity was observed. Thus, Fig. 8 presents the ASF plots for higher temperature obtained from increased water partial pressure in the cooling system. An enhanced production of alkanes between C_{10} and C_{20} at higher temperature and an average carbon chain length increase for lower temperatures in C_{21+} can be found. This trend is also confirmed by the gas phase, i.e., improved C_{5+} selectivity with decreasing temperature in Tab. 6.

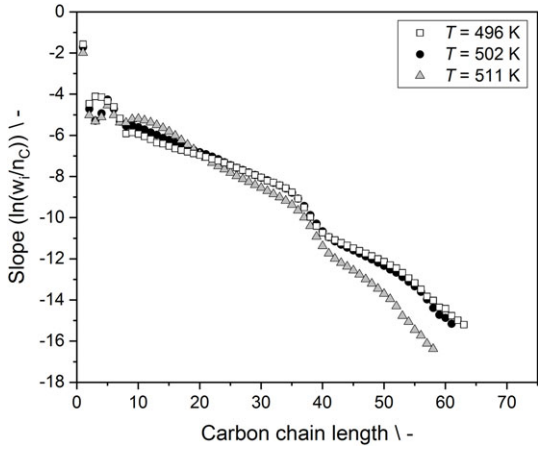

Figure 8. ASF plots at different reaction temperatures for experiments 2A–2C with respective temperatures of 496 K, 502 K, and 511 K in the pilot-scale reactor.

3.6 *WHSV* Variation in Pilot Scale

In Fig. 9, the *WHSV* influence is demonstrated for two different sets of parameters. The values of the *WHSV* were relatively high. Thus, the observable difference in the ASF plots is rather small. A lower *WHSV* value should increase the average chain length visibly. Interestingly, the maximum chain length seems not to be affected, again possibly due to high overall dilution.

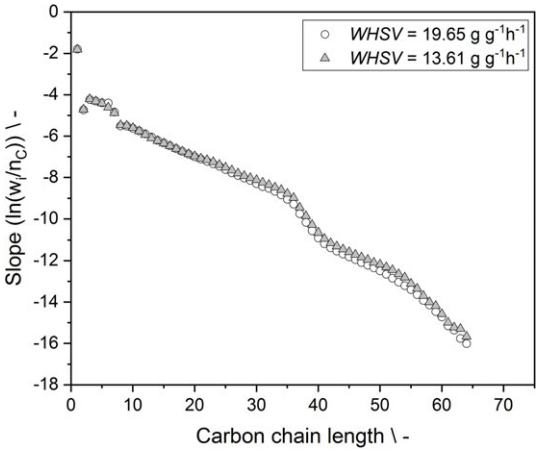

Figure 9. ASF plots with different *WHSV* from experiment 2D (*WHSV* = 19.7 g $g^{-1}h^{-1}$) and 2E (*WHSV* = 13.6 g $g^{-1}h^{-1}$) in the pilot-scale reactor.

In the end, a constant system performance and high load flexibility are apparent from these results, which is beneficial for any BtL application.

3.7 Success of Upscale

Experiments 1A and 2C enable a comparison of both reactor performances, since a similar temperature, residence time, and CO partial pressure was arranged. Only the syngas ratio differs with 1.91 vs. 1.72, because both setups were originally planned to compare parameters within the same reactor scale. Due to the high dilution, the effect of this difference on the reaction outcome should be limited, as discussed in Sect. 3.4. Regarding this, a comparison of both setups should be applicable.

In Fig. 10, the ASF plot for 1A (lab scale) and 2C (pilot scale) is displayed. While maintaining a similar CO conversion and productivity, the chain length of linear products in the larger reactor scale was observed. Between C_{10} and C_{25}, the form of the plots is similar. Differences in the curves between C_5 and

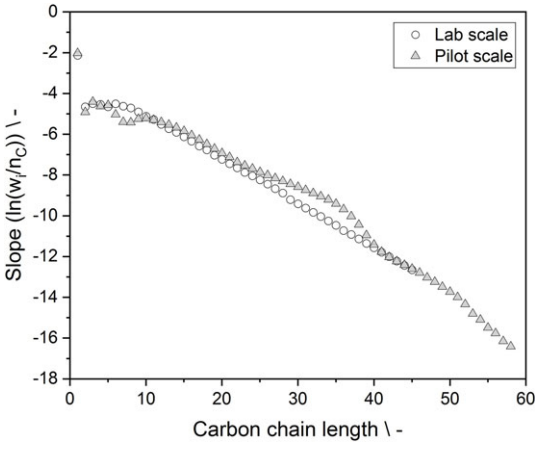

Figure 10. ASF plots for two comparable setups (1A and 2C) for both reactor scales.

C_{10} could be explained from variations in trap draining between the two reactor dimensions. Light hydrocarbons can potentially evaporate due to draining under ambient conditions. This was found in all experiments in pilot vs. lab scale. The means to cool down the sampling vessel while draining did not improve the lack of C_5 to C_{10}.

Both reactors use a similar core technology. The distribution of the feed gas as well as the layout and the mechanism behind the cooling structures are quite different, though. Both showed near isothermal behavior and comparable product quality for many different applications despite versatile experimental parameters. In conclusion, the successful upscale considerably benefits from evaporation cooling as means for high-pressure steam export. This system can be utilized quite easily in larger reactor scales. No apparent downsides could be observed that might have been caused by the upscale.

4 Conclusions

Flexibility towards different sources of syngas is an important characteristic of process applicability. With significantly improved reactor concepts, it seems possible to produce high-performance synthetic fuels in a decentralized and renewable manner. The BtL route typically provides a more challenging syngas quality compared to other sources but its potential is too high to be neglected. To demonstrate the versatility of microstructured reactors for the Fischer-Tropsch synthesis in decentralized applications, a reactor upscale (scaling factor of about 60) was investigated with a number of experimental parameters adjusted to BtL application.

It could be demonstrated that both reactor sizes achieve comparable conversion levels, especially regarding the high dilution of up to 56 % representing gasification using air. The performance would increase with less dilution to reach even higher conversions. This could be shown for undiluted setups in pilot scale. The total productivity typically reached acceptable values of 0.5–0.75 g $g_{cat}^{-1}h^{-1}$, while the productivity ratio of "oil" to "wax" as a function of the respective condensation temperatures was quite constant at 4:1. Product selectivity ranged from 10 to 18 mol % for methane with a selectivity towards higher hydrocarbons of 66–83 mol %.

Regarding long-term stability, the commercial cobalt catalyst showed no signs of rapid deactivation within the course of 1000+ h of experiment. Isothermal properties of the lab reactor were satisfying with a maximum temperature gradient of 2 K over the reactor length. This isothermal behavior was successfully transferred into the pilot reactor with typically 1–2 K temperature gradient using evaporation of water in special cooling structures. The reaction temperature has been effectively manipulated by adjustment of the water pressure in all cases.

The quality of the liquid product (FT oil) was comparable in all experiments and both reactors with a typical ratio of 4:1:1 for alkanes:alkenes:iso-alkanes which is quite promising for decentralized fuel production and distribution. The maximum chain length detected in the FT wax was 6 C-atoms, which is limited by the high gas dilution.

FT synthesis in microstructured reactors has been proven as pressure-tolerant between 1.5 and 3 MPa. Also, the H_2/CO

ratio under BtL-typical feed gas dilution showed no significant effect on the average chain length. Thus, the tradeoff between different types of syngas conditioning as well as gasification options can be weighed almost without consideration of the FT stage in case of a microstructured reactor.

The temperature increase in pilot scale followed a clear trend towards higher conversion at almost stable product distribution which is quite a singularity reached by the reactor design, as reported before [28, 29]. The low tendency towards deactivation at high conversion in highly diluted syngas raises hope towards a single-pass reactor operation in the FT process with satisfying results.

The comparison of microstructured FT reactors between lab scale and pilot scale has been investigated regarding the product quality. Insignificant changes from the scale-up in regard to product quality and reaction performance are evened out by improved controlling tools and operation mechanisms. This opens up scenarios for decentralized BtL or PtL applications. With an autothermal operation starting at a heat output only as low as 500 W allows quick temperature manipulation through water pressure adjustment which is a unique feature dedicated to PtL applications. Steam export enables the coupling of processes such as steam reforming, steam gasification, WGS, a steam turbine, or a steam electrolyzer to increase considerably the thermal efficiency of sector coupling.

Acknowledgment

The Vector Foundation is acknowledged for financial support of parts of this work within the DynSyn project. Additionally, parts of this work have been financially funded by the Young Innovators program ("Junge Innovatoren") of the Ministry of Science, Research and the Arts of the State of Baden-Wuerttemberg, Germany, as well as by the German Federal Ministry of Economy and Energy and the ESF (European Social Fund) Germany within the EXIST Business Start-up Grant ("EXIST Forschungstransfer", grant agreement No. 03EUGBW118). The authors like to thank the colleagues from KIT's Institute of Catalysis Research and Technology (IKFT) for enabling and supporting the wax analysis.

The authors have declared no conflict of interest.

Symbols used

a	[–]	slope of a linear curve
H	[kJ mol^{-1}]	enthalpy
m	[g]	mass
$\dot{m}$	[g h^{-1}]	mass flux
P	[g g$_{cat}^{-1}$h^{-1}]	specific productivity
p	[MPa]	pressure
S_{Ci}	[mol %]	selectivity towards species C_i
T	[K]	temperature
t	[h]	time
TOS	[h]	time-on-stream
$WHSV$	[g g$_{cat}^{-1}$h^{-1}]	weight hourly space velocity
w_i	[wt %]	mass fraction of species i
X_i	[vol %]	conversion of species i
y_i	[–]	gas fraction of species i

Greek letter

α	[%]	probability of chain growth

Sub- and superscripts

R	reaction
0	standard
C_{5+}	molecules with five carbon atoms or more
cat	catalyst
total	total amount

Abbreviations

ASF	Anderson-Schulz-Flory
ASU	air separation unit
BtL	biomass-to-liquid
CAD	computer-aided design
CHP	combined heat and power
CtL	coal-to-liquid
DME	dimethyl ether
FID	flame ionization detector
FTS	Fischer-Tropsch synthesis
GHG	greenhouse gas
GtL	gas-to-liquid
LTFT	low-temperature FT
MFC	mass flow controller
MFM	mass flow meter
MTG	methanol to gasoline
OME	oxymethylene ethers
PtL	power-to-liquid
SEM	scanning electron microscopy
TCD	thermal conductivity detector
WGS	water-gas shift
XtL	X-to-liquid

References

[1] F. Fischer, H. Tropsch, *Brennst. Chemie* **1923**, *4*, 276.
[2] M. Kousoulidou, L. Lonza, *Transp. Res. Part D* **2016**, *46*, 166. DOI: https://doi.org/10.1016/j.trd.2016.03.018
[3] *Greener Fischer-Tropsch Processes for Fuels and Feedstocks* (Eds: P. M. Maitlis, A. de Klerk), Wiley-VCH, Weinheim **2013**.
[4] S. Manabe, R. T. Wetherald, *J. Atmos. Sci.* **1967**, *24*, 241.
[5] http://www.worldbank.org/en/programs/zero-routine-flaring-by-2030 (Accessed on June 11, 2018)
[6] https://www.kopernikus-projekte.de/ (Accessed on June 11, 2018)
[7] A. Bisio, *Encyclopedia of Energy Technology and the Environment*, Wiley-Interscience, New York **1995**.
[8] A. Abu-Jrai, A. Tsolakis, K. Theinnoi, R. Cracknell, A. Megaritis, M. L. Wyszynski, S. E. Golunski, *Energy Fuels* **2006**, *20*, 2377.

[9] S. S. Gill, A. Tsolakis, K. D. Dearn, J. Rodríguez-Fernández, *Prog. Energy Combust. Sci.* **2011**, *37*, 503.
[10] https://www.umweltbundesamt.de/ (Accessed on July 03, 2018)
[11] https://www.bmwi.de/Redaktion/DE/Downloads/E/eeg-2017-fragen-und-antworten.pdf?__blob=publicationFile&v=20 (Accessed on February 12, 2019)
[12] M. J. A. Tijmensen, A. P. C. Faaij, C. N. Hamelinck, M. R. M. van Hardeveld, *Biomass Bioenergy* **2002**, *23 (2)*, 129. DOI: https://doi.org/10.1016/S0961-9534(02)00037-5.
[13] https://www.iea.org/renewables2018/ (Accessed on October 20, 2018)
[14] http://www.etipbioenergy.eu/images/EIBI-1-biomass-to-liquids.pdf (Accessed on October 20, 2018)
[15] R. Motal, Commercialization Considerations for Gas Conversion Technology Development, *ARPA-E Natural Gas Conversion Technologies Workshop*, Houston, TX, January **2012**.
[16] D. A. Wood, C. Nwaoha, B. F. Towler, *J. Nat. Gas Sci. Eng.* **2012**, *9*, 196.
[17] H. J. Venvik, J. Yang, *Catal. Today* **2017**, *285*, 135.
[18] http://www.chemie.de/news/1158952/treibstoff-fuer-klimaneutrales-fliegen.html (Accessed on February 20, 2019)
[19] https://soletair.fi/ (Accessed on June 11, 2018)
[20] https://www.comsynproject.eu/ (Accessed on June 11, 2018)
[21] C. N. Hamelinck, A. P. C. Faaij, H. den Uil, H. Boerrigter, *Energy* **2004**, *29*, 1743.
[22] S. Horvath, M. Fasihi, C. Breyer, *Energy Convers. Manage.* **2018**, *164*, 230.
[23] P. Schmidt, V. Batteiger, A. Roth, W. Weindorf, T. Raksha, *Chem. Ing. Tech.* **2018**, *90*, 127.
[24] *Fischer-Tropsch Technology* (Eds: A. Steynberg, M. Dry), Elsevier, Amsterdam **2004**.
[25] D. J. Wilhelm, D. R. Simbeck, A. D. Karp, R. L. Dickenson, *Fuel Process. Technol.* **2001**, *71*, 139.
[26] R. Dittmeyer, T. Boeltken, P. Piermartini, M. Selinsek, M. Loewert, F. Dallmann, H. Kreuder, M. Cholewa, A. Wunsch, M. Belimov, S. Farsi, P. Pfeifer, *Curr. Opin. Chem. Eng.* **2017**, *17*, 108. DOI: https://doi.org/10.1016/j.coche. 2017.08.001
[27] W. Bier, W. Keller, G. Linder, D. Seidel, K. Schubert, H. Martin, *Chem. Eng. Process. Process Intensif.* **1993**, *32*, 33.
[28] R. Myrstad, S. Eri, P. Pfeifer, E. Rytter, A. Holmen, *Catal. Today* **2009**, *147*, 301.
[29] P. Piermartini, T. Boeltken, M. Selinsek, P. Pfeifer, *Chem. Eng. J.* **2017**, *313*, 328. DOI: https://doi.org/10.1016/j.cej.2016.12.076
[30] C. Hopper, *J. Pet. Technol.* **2009**, *61*, 26.
[31] K. Ehrhardt, Micro Chemical Engineering – a fascinating journey from lab to industrial production, *IMRET 2018*, Karlsruhe, October **2018**.
[32] F. V. Vázquez, J. Koponen, V. Ruuskanen, C. Bajamundi, A. Kosonen, P. Simell, J. Ahola, C. Frilund, J. Elfving, M. Reinikainen, N. Heikkinen, J. Kauppinen, P. Piermartini, *J. CO2 Util.* **2018**, *28*, 235. DOI: https://doi.org/10.1016/j.jcou.2018.09.026
[33] S. LeViness, S. R. Deshmukh, L. A. Richard, H. J. Robota, *Top Catal.* **2014**, *57 (6–9)*, 518. DOI: https://doi.org/10.1007/s11244-013-0208-x
[34] The World Bank, *Mini-GTL Technology Bulletin*, The World Bank **2017**.
[35] http://www.neocarbonenergy.fi/ (Accessed on August 06, 2018)
[36] Velocys, *Presentation to analysts of the Oxford Catalysts Group* **2012**.
[37] S. LeViness, *Energy Frontiers International 2012*, Houston, TX, October **2012**.
[38] S. LeViness, *AIChE Spring Meeting*, San Antonio, TX, April/May **2013**.
[39] A. Faaij, B. Meuleman, R. van Ree, NOVEM Netherlands Agency for Energy and the Environment, *Long Term Perspectives of Biomass Integrated Gasification with Combined Cycle Technology: Costs and Efficiency and a Comparison with Combustion*, EWAB rapport, NOVEM **1998**.
[40] F. Dadgar, H. J. Venvik, P. Pfeifer, *Chem. Eng. Sci.* **2018**, *177*, 110. DOI: https://doi.org/10.1016/j.ces.2017.10.039
[41] M. E. Dry, *Catal. Today* **2002**, *71 (3–4)*, 227. DOI: https://doi.org/10.1016/S0920-5861(01)00453-9
[42] Ø. Borg, S. Eri, E. Blekkan, S. Storsater, H. Wigum, E. Rytter, A. Holmen, *J. Catal.* **2007**, *248 (1)*, 89. DOI: https://doi.org/10.1016/j.jcat.2007.03.008
[43] C. Knobloch, R. Güttel, T. Turek, *Chem. Ing. Tech.* **2013**, *85 (4)*, 455. DOI: https://doi.org/10.1002/cite.201200202
[44] C. Sun, T. Zhan, P. Pfeifer, R. Dittmeyer, *Chem. Eng. J.* **2017**, *310*, 272. DOI: https://doi.org/10.1016/j.cej.2016.10.118
[45] https://blog.restek.com/?p=10846 (Accessed on October 29, 2018)
[46] G. E. Totten, *Fuels and Lubricants Handbook: Technology, Properties, Performance, and Testing*, ASTM International, West Conshohocken, PA **2003**.
[47] *Fischer-Tropsch Technology* (Eds: A. Steynberg, M. Dry), Elsevier, Amsterdam **2004**.
[48] *Catalysis in the Refining of Fischer-Tropsch Syncrude* (Eds.: A. de Klerk, E. Furimsky), Royal Society of Chemistry, Cambridge **2010**.
[49] Deutsche Vereinigung des Gas- und Wasserfachs EV (DVGW), **2011**.
[50] A. Y. Khodakov, W. Chu, P. Fongarland, *Chem. Rev.* **2007**, *107 (5)*, 1692. DOI: https://doi.org/10.1021/cr050972v
[51] N. E. Tsakoumis, M. Rønning, Ø. Borg, E. Rytter, A. Holmen, *Catal. Today* **2010**, *154 (3–4)*, 162. DOI: https://doi.org/10.1016/j.cattod.2010.02.077
[52] M. Agee, *Fuel Technol. Manage.* **1997**, *7*, 69–72.
[53] J. van de Loosdrecht, B. Balzhinimaev, J.-A. Dalmon, J. W. Niemantsverdriet, S. V. Tsybulya, A. M. Saib, P. J. van Berge, J. L. Visagie, *Catal. Today* **2007**, *123 (1–4)*, 293. DOI: https://doi.org/10.1016/j.cattod.2007.02.032
[54] M. E. Dry, *J. Mol. Catal.* **1982**, *17 (2–3)*, 133. DOI: https://doi.org/10.1016/0304-5102(82)85025-6
[55] C. G. Visconti, E. Tronconi, L. Lietti, P. Forzatti, S. Rossini, R. Zennaro, *Top. Catal.* **2011**, *54 (13–15)*, 786. DOI: https://doi.org/10.1007/s11244-011-9700-3
[56] A. A. Adesina, *Appl. Catal., A* **1996**, *138 (2)*, 345. DOI: https://doi.org/10.1016/0926-860X(95)00307-X
[57] B. H. Davis, *Fischer-Tropsch Synthesis, Catalysts and Catalysis*, 1st ed., Studies in Surface Science and Catalysis, Vol. 163, Elsevier, Amsterdam **2007**.
[58] C. G. Visconti, M. Mascellaro, *Catal. Today* **2013**, *214*, 61. DOI: https://doi.org/10.1016/j.cattod.2012.10.016

[59] G. P. van der Laan, A. A. C. M. Beenackers, *Catal. Rev.* **1999**, *41 (3–4)*, 255. DOI: https://doi.org/10.1081/CR-100101170
[60] E. Rytter, A. Holmen, *Catalysts* **2015**, *5 (2)*, 478. DOI: https://doi.org/10.3390/catal5020478
[61] P. J. van Berge, R. C. Everson, in *Natural Gas Conversion IV*, 1st ed. (Eds: C. P. Nicolaides, M. D. Pontes, R. L. Espinoza), Studies in Surface Science and Catalysis, Vol. 107, Elsevier, Amsterdam **1997**.
[62] S. Rößler, C. Kern, A. Jess, *Chem. Ing. Tech.* **2018**, *90 (5)*, 634. DOI: https://doi.org/10.1002/cite.201700142
[63] T. Riedel, M. Claeys, H. Schulz, G. Schaub, S.-S. Nam, K.-W. Jun, M.-J. Choi, G. Kishan, K.-W. Lee, *Appl. Catal., A* **1999**, *186 (1–2)*, 201. DOI: https://doi.org/10.1016/S0926-860X(99)00173-8
[64] J. Yang, W. Ma, D. Chen, A. Holmen, B. H. Davis, *Appl. Catal., A* **2014**, *470*, 250. DOI: https://doi.org/10.1016/j.apcata.2013.10.061
[65] *VDI Heat Atlas*, V.D.I. VDI Gesellschaft Verfahrenstechnik und Ingenieurwesen, 2nd ed., Springer, Berlin **2010**.
[66] A. de Klerk, *Fischer-Tropsch Refining*, Wiley-VCH, Weinheim **2011**.
[67] H. Schulz, M. Claeys, *Appl. Catal., A* **1999**, *186 (1–2)*, 71. DOI: https://doi.org/10.1016/S0926-860X(99)00165-9

Research Article: A microstructured packed-bed reactor for the Fischer-Tropsch synthesis is investigated considering its versatility for biomass-based syngas with a high inert gas dilution. A 60 times larger pilot-scale reactor is further tested. Evaporation cooling is introduced which allows for enhanced energy extraction. From pilot scale, an autothermal operation at elevated conversion levels is applicable.

Microstructured Fischer-Tropsch Reactor Scale-up and Opportunities for Decentralized Application

M. Loewert*, J. Hoffmann, P. Piermartini, M. Selinsek, R. Dittmeyer, P. Pfeifer

Chem. Eng. Technol. **2019**, *42 (10)*, XXX … XXX

DOI: 10.1002/ceat.201900136